symmetry

MDPI

Article

Symmetry Analysis of the Complex Polytypism of Layered Rare-Earth Tellurites and Related Selenites: The Case of Introducing Transition Metals

Dmitri O. Charkin [1,2], Valeri A. Dolgikh [1], Timofey A. Omelchenko [1], Yulia A. Vaitieva [2], Sergey N. Volkov [2,3], Dina V. Deyneko [1,2] and Sergey M. Aksenov [2,4,*]

[1] Department of Chemistry, Lomonosov Moscow State University, GSP-1, 1-3 Leninskiye Gory, 119991 Moscow, Russia
[2] Laboratory of Arctic Mineralogy and Material Sciences, Kola Science Centre, Russian Academy of Sciences, Fersmana Str. 14, 184209 Apatity, Russia
[3] Grebenshchikov Institute of Silicate Chemistry, Makarov Emb, 199053 St. Petersburg, Russia
[4] Geological Institute, Kola Science Centre, Russian Academy of Sciences, 14 Fersman Street, 184209 Apatity, Russia
* Correspondence: aks.crys@gmail.com

Abstract: Our systematic explorations of the complex rare earth tellurite halide family have added several new $[Ln_{12}(TeO_3)_{12}][M_6X_{24}]$ (M = Cd, Mn, Co) representatives containing strongly deficient and disordered metal-halide layers based on transition metal cations. The degree of disorder increases sharply with decrease of M^{2+} radius and the size disagreements between the cationic $[Ln_{12}(TeO_3)_{12}]^{+12}$ and anionic $[M_6Cl_{24}]^{-12}$ layers. From the crystal chemical viewpoint, this indicates that the families of both rare-earth selenites and tellurites can be further extended; one can expect formation of some more complex structure types, particularly among selenites. Analysis of the polytypism of compounds have been performed using the approach of OD ("order–disorder") theory.

Keywords: polytypism; OD structures; rare-earth tellurium oxyhalides; stacking disorder; crystal chemistry; selenites

Citation: Charkin, D.O.; Dolgikh, V.A.; Omelchenko, T.A.; Vaitieva, Yu.A.; Volkov, S.N.; Deyneko, D.V.; Aksenov, S.M. Symmetry Analysis of the Complex Polytypism of Layered Rare-Earth Tellurites and Related Selenites: the Case of Introducing Transition Metals. *Symmetry* **2022**, *14*, 2087. https://doi.org/10.3390/sym14102087

Academic Editor: György Keglevich

Received: 4 September 2022
Accepted: 27 September 2022
Published: 7 October 2022

1. Introduction

The use of species with "one-sided" coordination which terminate propagation of the net of chemical bonds and contribute to interfaces with non-covalent interactions is a common and a powerful instrument in the construction of low-dimensional, porous, and open-framework inorganic structures for various purposes [1–6]. This approach employs either organic species with hydrophilic parts contributing to the frameworks and hydrophobic parts forming the interfaces, or cations with the stereoactive lone pair of electrons such as Tl^+, Sn^{2+}, Pb^{2+}, As^{3+}, Sb^{3+}, Bi^{3+}, Se^{4+}, Te^{4+}, or I^{5+} [2,5–9]. The interiors of the covalent frameworks may be filled by small anions, most commonly halides, or much larger ensembles, e.g., salt-inclusion solids [10]. Combinations of "lone-pair" and "regular-coordination" cations, particularly rare-earth and halide anions, often result in layered arrangements comprised of alternating covalent (metal-oxide) and ionic (metal-halide) 2D infinite building blocks bearing opposite charges [1]. They are more frequently observed among compounds containing rare-earth cations with isotropic coordination and Se^{IV} or Te^{IV} which form the interfaces of the cationic metal-oxide parts.

By now, the majority of their structures contain tetragonal or pseudo-tetragonal $[Ln_{11}M_n(ChO_3)_{12}]$ layers (Ch = Se or Te, M = Ln or some other uni- or divalent cations) sandwiched between either single halide sheets or more complex metal-halide slabs derived from tetragonal FeS (based on tetrahedrally coordinated Cu^+ or Zn^{2+} and Cl^- [11]),

CsCl (based on MX_8 cubes M = K, Rb and Cs; X = Cl or Br [10,12–15]) or NaCl (based on $CdCl_6$ or $CdBr_6$ octahedra [16,17]) as shown schematically in Figure 1. Octahedral coordination in halides is common also for some other transition metal dications including Mn^{2+}, Co^{2+}, and Ni^{2+}. Layered rare-earth-chalcogen (IV) oxyhalides containing magnetically active cations have been reported only for the $[Ln_{10}M(SeO_3)_{12}][Cl_8]$ composition with low amounts of M^{2+} at very large separations [11]. The possibility of constructing transition metal-rich building blocks within this family has not been explored to date; the only hint to their possible existence is given in [11] where a $[La_{11}(SeO_3)_{12}][Co_{7.5}Cl_{24}]$ composition is once mentioned without comments. This formula corresponds to that of the Cd compounds, $[Ln_{12}(TeO_3)_{12}][Cd_6X_{24}]$, X = Cl, Br [16,17] (Figure 1d); the ordered arrangement of the transition metal (Co^{2+} in this case) cations only within the metal-halide slabs is expected to result in formation of relatively dense planar or quasi-planar magnetic sublattices situated at relatively large (~13Å) separations.

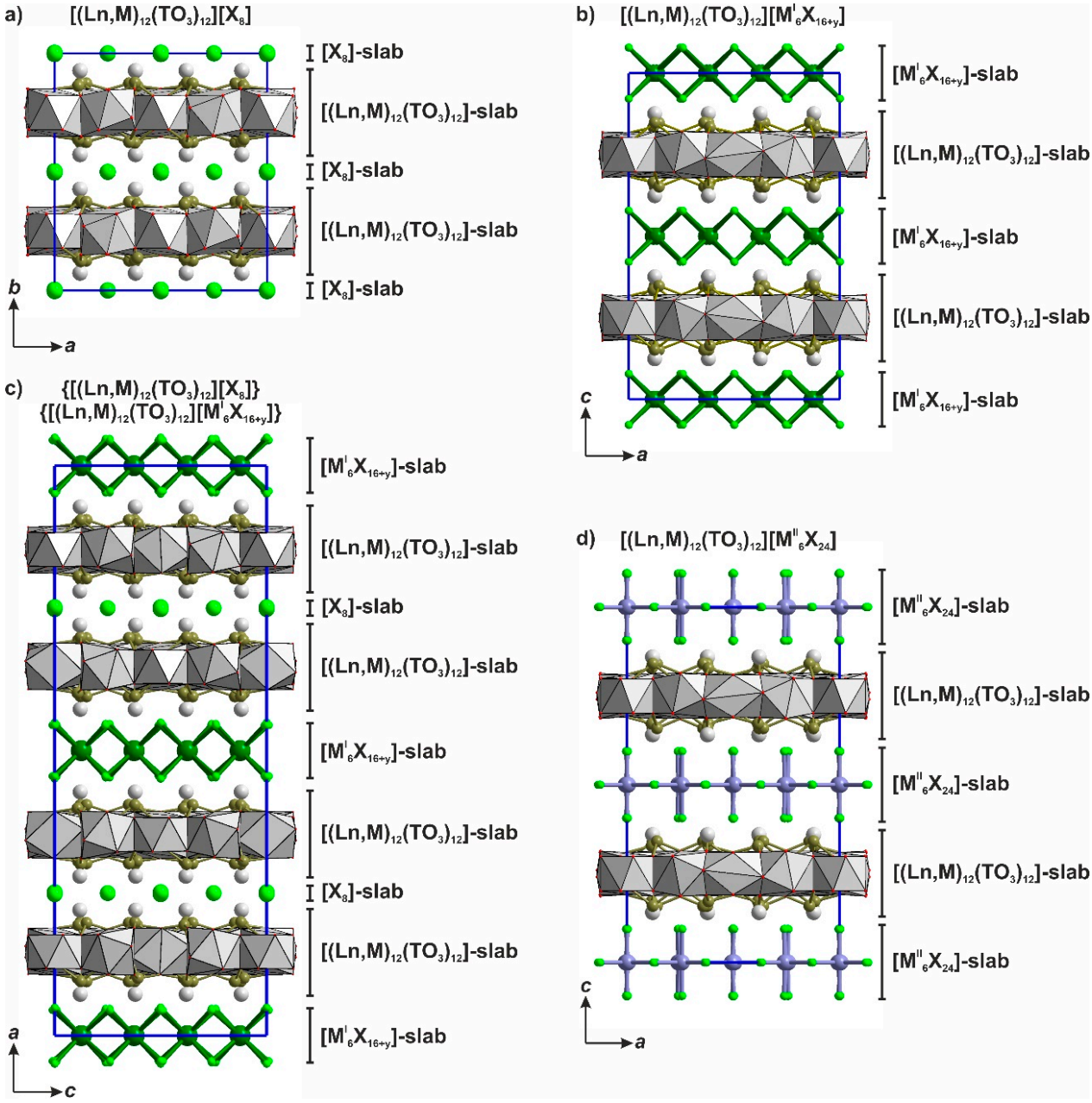

Figure 1. Different possible types of the alternations of $[(Ln, M)_{12}(TO_3)_{12}]^{n+}$ slabs with the $[X_8]$ slab (**a**), $[M^{I}X_{16+y}]$ slabs (**b**), both $[X_8]$ and $[M^{I}X_{16+y}]$ slabs (**c**) and $[M^{II}_6X_{24}]$ slabs (**d**).

For the modular compounds with the layered structures (with the weak interactions between the adjacent layers), the presence of the stacking disorder is very common [18]. The slight shifts can form different polytypes and OD ("order–disorder") structures [19–21]. The symmetry analysis of such disordered compounds is based on the concepts of OD theory [22,23] and the symmetry of the OD structures is described by groupoids (instead of crystallographic space groups), which can contain the non-crystallographic symmetry operations [24–26]. This approach allows to determine the symmetry relations for the whole family of known polytypes and predict the hypothetical ones [27], which is important for the searching of new materials [28–34]. The OD structures with the different polytypes have been also described for the tellurium compounds, in particular, for the hydrous magnesium orthotellurate (VI) $Mg(H_2O)_2[TeO_2(OH)_4]$ [35], copper–zinc oxotellurite (IV) $[Cu_2ZnTeO_4][SO_4 \cdot H_2O]$ [36], and alkali metal zinc oxidotellurites (IV), $Rb_2Zn(TeO_3)(CO_3)\cdot H_2O$ and $Na_2Zn_2Te_4O_{11}$ [37].

The presence of stacking disorders for the family of compounds containing tetragonal or pseudo-tetragonal $[Ln_{11}M_n(ChO_3)_{12}]$ layers have been recently reported based on the TEM images [38]. It was also mentioned that for the accurate description of the polytypes, the corresponding OD analysis is required [38]. Hereby, we report the results of our attempts to prepare such compounds; contrary to the Cd^{2+} based prototypes, they exhibit gross disorder in the targeted M^{2+} sublattices, which could be plausibly modeled in just a few cases. A new representative was also obtained for the family of Ln-Cd tellurite halides; its structure was refined to quite reasonable values and will be described here as a "best ordered" reference structure. The accurate symmetry analysis for these compounds using the approach of OD theory is given and polytypic relations have been determined.

2. Materials and Methods

2.1. Synthesis

As in the previous reports [10,15–17], the starting compounds were LnOX, TeO_2, and MX_2 (M = Mn, Co, Ni). Anhydrous Co and Mn compounds obtained from MnX_24H_2O and CoX_26H_2O via dehydration by gentle heating (up to ~100 °C) and subsequent cooling *in vacuo* (down to ca. 50–70 Pa). Anhydrous nickel halides were prepared in the same way starting from NiX_26NH_3. The anhydrous halides were pink (MnX_2), deep blue ($CoCl_2$), deep green ($CoBr_2$), yellow ($NiCl_2$) and brown ($NiBr_2$). Due to high hygroscopicity of CoX_2, all operations with these compounds were conducted in an argon-filled glovebox. The halides of Mn and Ni permit handling in air for a short time. Mixtures of LnOX, MX_2, and TeO_2 in 1:7:1 ratio were ground, placed in silica capsules, gently heated in a dynamic vacuum until the pressure dropped to ca. 50 Pa, sealed, and annealed according to the following scheme: heating to 600 °C within 12 h, plateau 12 h; heating to 850 °C within 12 h, plateau 120 h; cooling to 650 °C within 120 h. The salt fluxes were dissolved in water (Ni and Mn halides) or 96% ethanol (Co halides). The insoluble residues consisted of small colorless, pinkish (Mn) or deep blue (Co) crystals. Suitable crystals were not produced using NiX_2. The novel Ce-Cd-Te oxychloride was obtained as a somewhat unexpected product from a mixture of $SrTeO_3$, CeOCl, TeO_2, $SrCl_2$, and $CdCl_2$ (1:1:1:3:4) targeted at a different proposed composition. It is reported here as it belongs to the same structural family.

2.2. Diagnostics

Single crystals of the Co compounds were characterized by energy-dispersive X-ray spectroscopy using a Leo Supra 50 VP electron microscope utilizing 15 kV accelerating voltage and an INCA analyzer. The results indicate that two kinds of crystals were observed in the Eu and Gd-containing samples: those containing only Ln, Te, and Cl, as well as those also containing Co. In the bromide sample, only blue crystals have been studied which were shown to contain La, Co, Te, and Br.

2.3. Single Crystal X-ray Analysis

Though formation of relatively large platelets or respective colors was observed in a variety of samples, even examination in an optical microscope showed most of them then to be piles of very thin foil-like sheets, sometimes with uneven coloring. Acceptable quality crystals were observed for M^{2+} = Cd, X = Cl, Ln = Ce (**1**), M^{2+} = Mn, X = Cl, Ln = Nd (**2**), M^{2+} = Mn, X = Br, Ln = La (**3**), M^{2+} = Co, X = Cl, Ln = Eu (**4**), and M^{2+} = Co, X = Cl, Ln = Gd (**5**). Single crystals found in the La-Co-Te-O-Br sample were of too low quality and were not studied. The others were selected under a polarizing microscope for single-crystal X-ray diffraction. The single-crystal X-ray data were collected on a Rigaku XtaLAB Synergy diffractometer (HyPix detector, MoK_α radiation, λ = 0.71073 Å; ω−θ-scanning mode) (**1**), Bruker SMART APEX II diffractometer (CCD detector; MoK_α radiation, λ = 0.71073 Å; ω−θ-scanning mode) (**2**,**3**), and Xcalibur S Oxford Diffraction diffractometer (CCD detector; MoK_α radiation, λ = 0.71073 Å; ω−θ-scanning mode) (**4**,**5**). Raw data were integrated and then scaled, merged, and corrected for Lorentz-polarization effects using the CrysAlis [39] and Apex2 [40] programs. A semiempirical absorption correction based upon the intensities of equivalent reflections was applied using SADABS [41].

The observed single-crystal diffraction patterns indicated the bad quality of studied crystals which was typically manifested by essential streaking (indicating stacking disorder) and poorly resolved reflections. In accordance with the analysis of systematic absence of reflections, the space group *P*4/*nbm* (No. 125) for all compounds was chosen. The experimental details of the data collection and refinement results are also listed in Table 1.

Table 1. Crystal data, data collection, and refinement of grown crystals.

Sample Number	**$[Ce_{12}(TeO_3)_{12}][Gd_6Cl_{24}]$ (1)**	**$[Nd_{12}(TeO_3)_{12}][Mn_6Cl_{24}]$ (2)**	**$[La_{12}(TeO_3)_{12}][Mn_6Br_{24}]$ (3)**	**$[Eu_{12}(TeO_3)_{12}][Co_6Cl_{24}]$ (4)**	**$[Gd_{12}(TeO_3)_{12}][Co_6Cl_{24}]$ (5)**
Molecular weight (g)	5321.5	5014.3	5978.4	5135.4	5198.4
Temperature (K)	293				
Cell setting	Tetragonal				
Space group	*P*4/*nbm* (125)				
a (Å)	16.3262 (1)	16.0692 (11)	16.4400 (49)	15.8928 (6)	15.8323 (7)
c (Å)	13.0257 (1)	12.6796 (9)	13.5077 (40)	12.4614 (13)	12.4729 (1)
V (Å^3)	3471.93 (4)	3274.12 (4)	3650.77 (3)	3147.5 (4)	3126.46 (3)
Z	2				
Calculated density, D_x (g cm^{-3})	5.0902	5.086	5.438	5.418	5.522
Crystal size (mm)	0.02 × 0.06 × 0.08	0.01 × 0.03 × 0.06	0.03 × 0.04 × 0.07	0.03 × 0.05 × 0.08	0.08 × 0.10 × 0.12
Crystal form	Anhedral grain	Anhedral grain	Anhedral grain	Anhedral grain	Anhedral grain
Crystal color	yellowish	lilac	pink	deep blue	deep blue
Data collection					
Diffractometer	Rigaku XtaLAB Synergy (HyPix detector)		Bruker Apex II (CCD detector)	Xcalibur S Oxford Diffraction (CCD detector)	
Radiation; λ	Mo$K\alpha$; 0.71073				
Absorption coefficient, μ (mm^{-1})	15.368	16.696	25.496	19.839	20.664
F (000)	4615	4377	5134	4476	4500
Data range θ(º); *h*, *k*, *l*	3.2–33.39; −18 < *h* < 24, −25 < *k* < 24, −19 < *l* < 20	2.41–30.25; −22 < *h* < 22, −22 < *k* < 13, −16 < *l* < 17	2.31–30.32; −23 < *h* < 22, −23< *k* < 23, −18 < *l* < 19	3.30–35.37; −17 < *h* < 25, −25 < *k* < 24, −19 < *l* < 19	3.31–35.39; −24 < *h* < 24, −24 < *k* < 15, −19 < *l* < 14
No. of measured reflections	46,388	16,881	34,403	32,931	32,476
Total reflections (N_2) /observed (N_1)	3194/2957	2314/1937	2625/1204	3432/1093	3411/1052

Criterion for observed reflections	$I > 3\sigma(I)$				
R_σ/R_{int} (%)	0.96/3.4	2.95/4.68	9.77/ 2.98	12.24/22.13	11.50/21.46
Refinement					
Refinement on	Full-matrix least squares on F	Full-matrix least squares on F	Full-matrix least squares on F	Full-matrix least squares on F^2	Full-matrix least squares on F^2
Weight scheme	$1/(\sigma^2\|F\| + 0.0004F^2)$	$1/(\sigma^2\|F\| + 0.0004F^2)$	$1/(\sigma^2\|F\| + 0.0004F^2)$	$1/(\sigma^2\|I\| + 0.0036I^2)$	$1/(\sigma^2\|I\| + 0.0064I^2)$
R_1, wR_2 (all reflection) (%)	3.65/6.01	4.03/5.64	6.29/8.27	5.74/20.58	6.26/24.03
GOF (Goodness of fit) (%)	2.47	1.75	1.14	1.02	1.04
Max./min. residual e density, (eÅ^{-3})	9.58/−5.00	3.99/−5.22	10.27/−5.51	6.97/−6.44	9.15/−5.15
CCDC Number	2202776	1974365	2202775	1939966	1939965

Structure models were determined by the "charge flipping" method using the SUPERFLIP computer program [42] and were refined using the JANA2006 computer program [43]. Illustrations were produced with the JANA2006 program package in combination with the DIAMOND program [44]. Atomic scattering factors for neutral atoms together with anomalous dispersion corrections were taken from International Tables for Crystallography [45]. These essential values of $\Delta\rho_{min}$ and $\Delta\rho_{max}$ are most likely the result of stacking faults common for the layered structures and indicating their possible OD character that was also manifested by streaks in the diffraction patterns. Similar problems, though slightly less pronounced, were encountered in some previous studies [15–17]. Attempts to split the corresponding sites were not successful, leading mostly to non-positive definite sites, and were finally abandoned. Tables S1 list fractional site coordinates and equivalent displacement parameters for 1 to 5. Selected bond distances are given in Table S2. CCDC 1939965, 1939966, 1974365, 2202775, 2202776 contain the supplementary crystallographic data for these compounds. The data can be obtained free of charge from The Cambridge Crystallographic Data Centre via www.ccdc.cam.ac.uk/structures.

3. Results

3.1. Crystal Structure Description

The crystal structures of the studied compounds **1–5** are similar to the previously studied ones with the space group *P*4/*nbm* (Figure 1d) Their crystal structures contain two blocks which alternate along *c* parameter. The first block is represented by a complex slab formed by edge-shared Lnφ_n-polyhedra (n = 8–12) with the general formula $[Ln_{12}(TeO_3)_{12}]$ (type B slab [17]) (Figure 2), where Ln = La, Ce, Nd, Eu, and Gd. The second slab is represented by three-layered close-packing formed by the halide X^- anions (X = Cl or Br) with octahedral sites occupied by the M^{2+} cations (M = Mn, Co, Cd).

In the crystal structures of compounds **1–5**, the $[Ln_{12-x}(TeO_3)_{12}]$ type B slabs are nearly identical, with differences in bond lengths due to the varied size of Ln^{3+} cations. In the $[M^{II}_{6+y}X_{24}]$ blocks, the M^{2+} cations fill the octahedral voids; however, refinement of the corresponding site occupancies and analysis of the electron density maps for **1–3** indicate presence of maxima which we interpret as the additional weakly occupied M sites (close to the main ones) (Figure 3a). The statistical distributions of M^{2+} cations within the octahedral cavities lead to the formation of two types of the layers characterized by the different orientations of octahedra (Figure 3b,c).

The final refinement cycles converged to reasonable values for **1** and **2**; however, an ordered model could be refined only for **1**. In the structure of **2** and particularly of **3–5**, occupancies of octahedrally coordinated M^{2+} positions (M^{2+} = Mn, Co) were evidently below unity; in addition, relatively high electron density peaks were found in different Fourier maps. Some of these could be tentatively assigned to additional weakly occupied M^{2+} sites. This is another clear manifestation of the OD character of the structures.

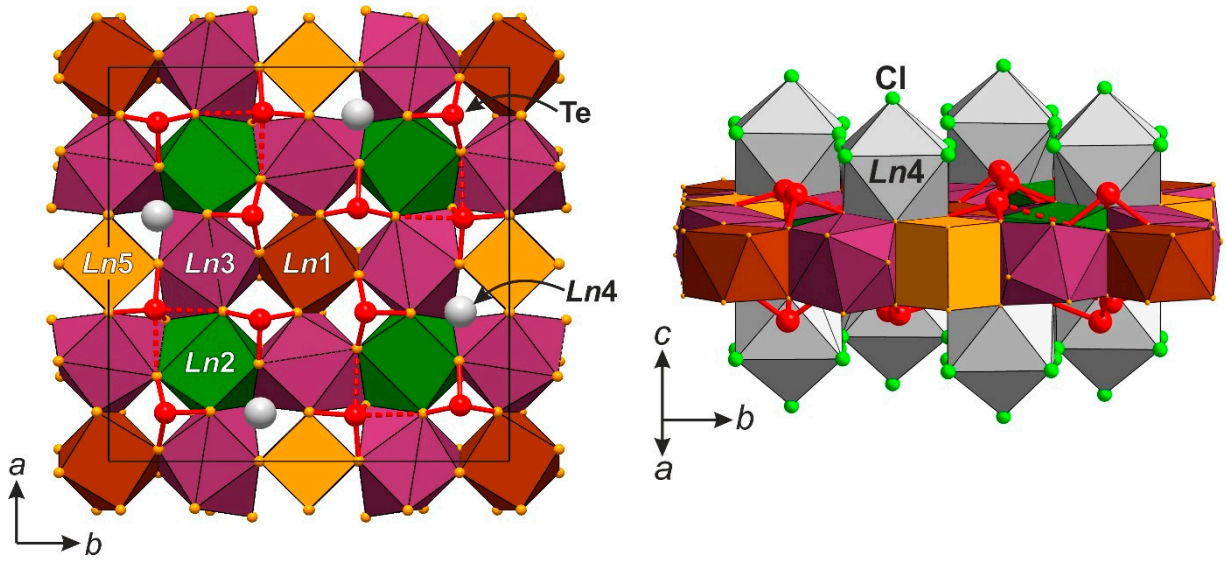

(**a**) (**b**)

Figure 2. The general views of the $[Ln_{12-x}(TeO_3)_{12}]$ type slab projected on (001) (**a**) and the same slab with the "outer" $Ln4\varphi_n$ polyhedra (**b**) in the crystal structures of compounds with the general formula $[Ln_{12}(TO_3)_{12}][M_6X_{24}]$, where M = Cd, X = Cl, Ln = Ce (compound **1**), M= Mn, X = Cl, Ln = Nd (**2**), M = Mn, X = Br, Ln = La (**3**), M = Co, X = Cl, Ln = Eu (**4**), and M = Co, X = Cl, Ln = Gd (**5**).

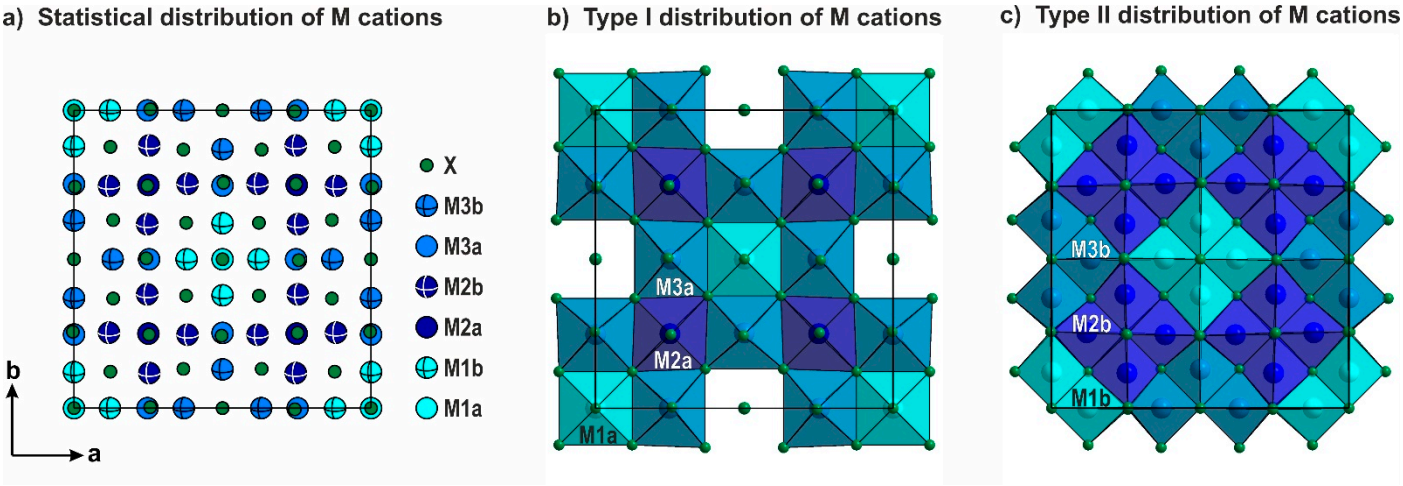

Figure 3. Different types of distribution of M cations within the $[M_6X_{24}]$ layer: the statistical disordered arrangement (**a**) and ordered types (**b**,**c**).

3.2. Polytypism of Tetragonal Halides Containing the $[Ln_{12}(TO_3)_{12}]$ Slabs

The diffraction patterns of tetragonal layered rare-earth tellurite halogenides [16,17] are typically characterized by a remarkably low quality of the single crystal X-ray diffraction data which indicates the presence of various stacking faults and possibly some other 2D defects such as single halide sheets. Within the family of related compounds (Figure 1), there are two types of the structures with the following unit cell parameters: *a*~15.77–16.44 Å, *c*~12.92–13.77 Å (sp. gr. *P*4/*nbm*, *Z* = 2) and *a*~15.80–16.12 Å, *c*~24.82–26.41 Å (sp. gr. *I*4/*mcm*, *Z* = 4). The doubling of the *c* parameter of the unit cell is observed predominantly for compounds with M^I = alkali cation (K, Rb, Cs) with the $[M^I_6X_{16}]$ composition of the layer (the only exception is compound $[Gd_{12}(TeO_3)_{12}][Cd_6Cl_{24}]$ [16]).

Taking into account the layered type of the structures as well as different possible ways of their linkage, the observed structural variants can be considered as polytypes

[18,46]. The presence of the twinning indicates the possible stacking disorder and OD ("order–disorder") [47,48] character of the structures. The crystal structures of compounds with the general formulas $[Ln_{12}(TeO_3)_{12}][M^{II}_6X_{24}]$ and $[(Ln,M^{I})_{1-x}Ln_{11}(TeO_3)_{12}][M^{I}_6X_{16+y}]$ [15] can be described using the same OD groupoid family, more precisely, a family of OD structures built up by two kinds of non-polar layers (category IV) [49]. The layers are the following (Figure 4a,b):

(i) L_{2n} type with layer symmetry $p4/nmm$ [or $P(4/n)mm$ in the terms of OD notation] is formed by $[M_6X_{24}]$, $[M_6X_{16}]$ or $[X_8]$ layer (Figure 4b).

(ii) L_{2n+1} type with layer symmetry $p4/nbm11$[or $P(4/n)bm$ in terms of the OD notation, where braces in the third position indicate the direction of missing periodicity [50]] is formed by a $[Ln_{12}(TeO_3)_{12}]$ type B slab (Figure 4a).

The layers of both types (L_{2n} and L_{2n+1}) alternate along the ***c*** direction and have common translation vectors *a* and *b*, with c_0, the distance between the two nearest equivalent layers, corresponding to $(c/2)$~6.6 Å. The ordered or disordered alternation of the two kinds of layers gives rise to a whole family of ordered polytypes or disordered sequences, which can be obtained through the action of the following symmetry operators that may be active in the L_{2n}-type of layer: the 2 and 2_1 axes parallel to a ([2 1 1] or [2_1 1 1]) and/or b ([1 2 1] or [1 2_1 1]). The symmetry relation common to all polytypes of this family are described by the OD groupoid family symbol:

$$\begin{matrix} P\left(\frac{4}{m}\right)mm & & P\left(\frac{4}{n}\right)bm \\ & [r,s] & \end{matrix} \quad (1)$$

where the first line contains the layer-group symbols of the two constituting layers, while the second line indicates the positional relations between the adjacent layers [51].

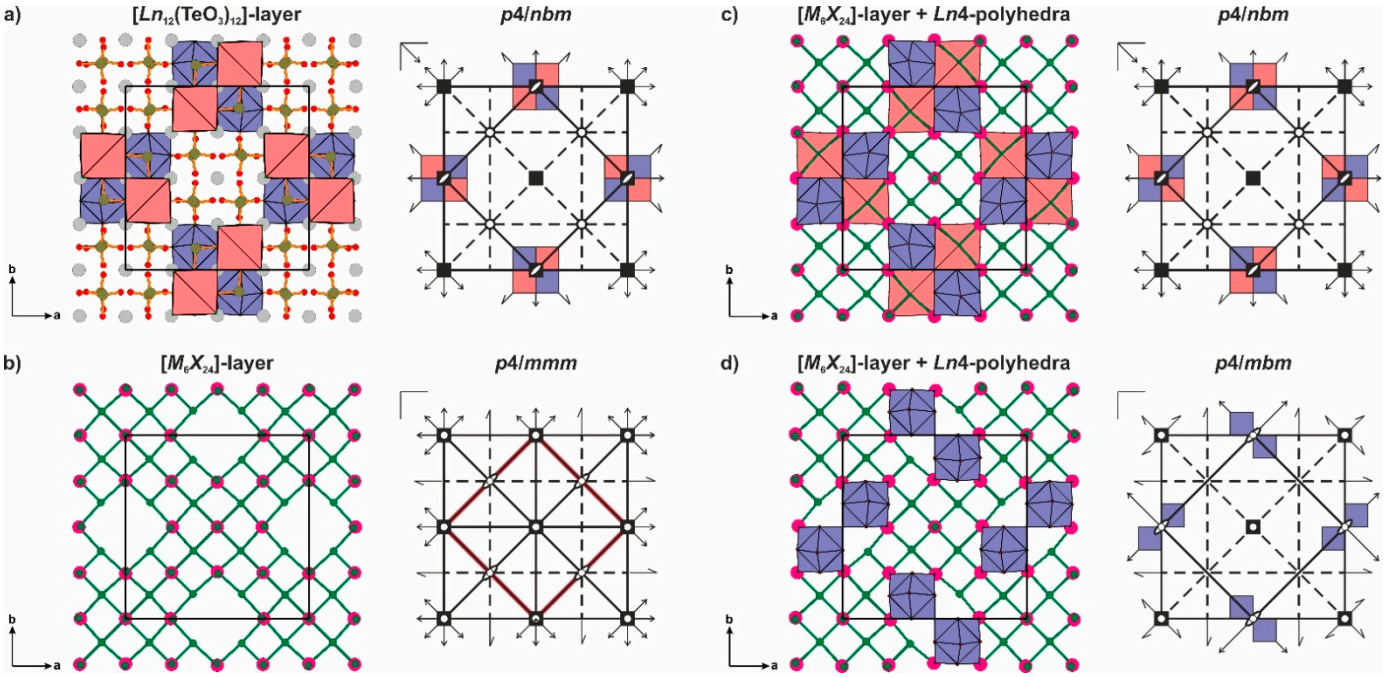

Figure 4. The general views and the symmetry of the L_{2n+1} (**a**) and L_{2n} (**b**) OD-layers crystal structure of compounds with the general formula $[Ln_{12}(TeO_3)_{12}][M_6X_{24}]$ and $[(Ln,M^{I})_{1-x}Ln_{11}(TeO_3)_{12}][M^{I}_6X_{16+y}]$. The different types of the arrangements of Ln4-polyhedra of L_{2n+1} layers across the L_{2n} layer and the symmetry of the triplets L_{2n-1},L_{2n},L_{2n+1} observed in the crystal structures of MDO1-polytype (with the space group $P4/nbm$) (**c**) and MDO2-(**d**) polytype (with the space group $I4/mcm$) are shown.

In all the polytypes, as well as in the disordered sequences, pairs of adjacent layers are geometrically equivalent (according to the general principle of OD structures). Polytypes presenting the smallest possible number of different triples of layers are called MDO (Maximum Degree of Order) polytypes (the principle of MDO structures). The first MDO structure (MDO1-polytype) can be obtained when the 2_x and 2_y axes are active in the $L2_n$-type layers (Figure 4c), giving the tetragonal structure with *a*~16.0 Å, *c*~13.2 Å and the space group *P*4/*nbm*. The second MDO structure (MDO2-polytype) can be obtained when the 2_{1x} and 2_{1y} axes are active in the $L2_n$-type layers: *a*~16.0 Å, *c*~25.5 Å and the space group *I*4/*mcm*.

The similar stacking disorder with the formation of different types of polytypes have been also previously observed for the related rare-earth selenites [12,13,38,52–55]. The crystal structures of $[LiPr_{11}(SeO_3)_{12}][Rb_6Cl_{16}]$ [13] and $[LiNd_{11}(SeO_3)_{12}][Rb_6Cl_{16}]$ [12] are crystal chemical isotypical [56] to tellurites with the general formula $[(Ln,M^I)_{1-x}Ln_{11}(TeO_3)_{12}][M^I_6X_{16+y}]$ [15] and are represented by the MDO1-polytype with the space group *I*4/*mcm*.

In the crystal structures of $[M^{II}Nd_{10}(SeO_3)_{12}][Cl_8]$ (M^{II} = Ca, Sr; Figure 1a) [52] and $[Cs_{0.5}Sm_{10.5}(SeO_3)_{12}][Br_8]$ [55] the type B slabs are linked directly via a single-layered $[X_8]$ block (X = Cl, Br), forming the heteropolyhedral framework. Despite the reduced interstitial $[X_8]$ block represented only by a single layer with the one atom width the polytypic character remains common for the whole family of compounds. Compounds $[MNd_{10}(SeO_3)_{12}][Cl_8]$ (M = Ca, Sr) [52] and $[Cs_{0.5}Sm_{10.5}(SeO_3)_{12}][Br_8]$ [55] are crystal chemical isotypical and represent the third type of MDO structure (MDO3-polytype). This polytype can be obtained when the 2_{1x} and 2_y axes are active in the $L2_n$-type layers (Figure 5a) giving the orthorhombic (pseudo-tetragonal) structure with *a*~15.7 Å, *a*~15.7 Å *c*~17.9 Å and the space group *Bbab* (non-standard setting of the space group *Ccca*).

Compounds $[Sm_{11}(SeO_3)_{12}][K_7Cl_{16}]$ [54] and $[Nd_{11}(SeO_3)_{12}][Cs_7Cl_{16}]$ [38] are characterized by another MDO structure (MDO4-polytype) which can be obtained when the 2_y axes are active in the $L2_n$-type layers (Figure 5b) giving the orthorhombic (pseudo-tetragonal) structure with *a*~15.7 Å, *a*~15.7 Å *c*~17.9 Å and the space group *Pnan*. For the compound $[Nd_{11}(SeO_3)_{12}][Cs_7Cl_{16}]$ [38], symmetry lowering was confirmed by a second harmonic generation test, and the space group $Pna2_1$ (which is a subgroup of the space group *Pnan*) was established. It needs be noted that among selenites, one site in the type B layer is mostly empty while on the CsCl layer, one additional cubic void is occupied instead by a voluminous alkali cation.

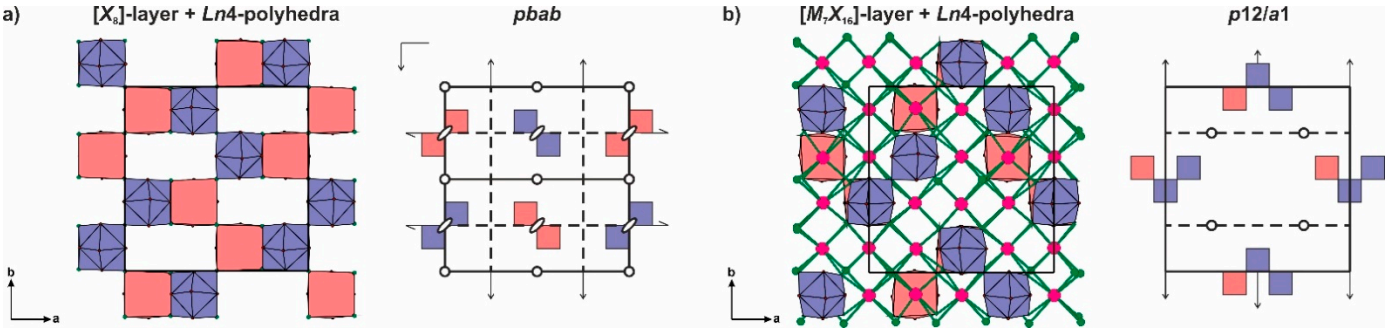

Figure 5. The different types of the arrangements of Ln4-polyhedra of $L2_{n+1}$ layers across the $L2_n$ layer and the symmetry of the triplets $L2_{n-1}$,$L2_n$,$L2_{n+1}$ observed in the crystal structures of MDO3-polytype (with the space group *Bbab*) (**a**) and MDO4-polytype (with the space group *Pnan*) (**b**).

When different sequences of operators are active in the $L2_n$-type layers, multilayered non-MDO polytypic structures with increased **c** occur. The simplest ones are those in which the two types of operators in $L2_n$ layers regularly alternate. The crystal structures of $[Pr_{11}(SeO_3)_{12}][Cs_7Cl_{16}]$ [54] and $[Nd_{11}(SeO_3)_{12}][Cs_7Cl_{16}]$ [38] with the orthorhombic (pseudo-tetragonal) unit cell parameters *a* = 15.9, *b* = 15.9, *c* = 51.6 Å and the space groups *Cmce* or

Pban are unknown, but the TEM images of $[Nd_{11}(SeO_3)_{12}][Cs_7Cl_{16}]$ [38] show the regular stacking disorder and different kinds of symmetrical operation active in L_{2n}-type layers.

Except for different MDO and non-MDO structures, the modular structures can also be formed when the different types of the interstitial block between adjacent $[Ln_{12}(TeO_3)_{12}]$ type B slab are present. As a result, the different types of alternation can form a merotypic modular series [18,33,46,57–59]. In the crystal structure of $[La_{11}(SeO_3)_{12}]_2[Cs_6Cl_{16}][Cl_8]$ [53], there are four type B slabs, two $[M^I_6X_{16}]$ blocks and two $[X_8]$ blocks, and the crystal chemical formula can be written as $\{[La_{11}(SeO_3)_{12}]^{+9}[Cs_6Cl_{16}]^{-10}\}^{-1}\{[La_{11}(SeO_3)_{12}]^{+9}[Cl_8]^{-8}\}^{+1}$. Such complex structure is relatively strictly ordered as only the whole layer sequence is electroneutral. The same applies to the compounds $\{[La_{11}(SeO_3)_{12}]^{+9}[Cu_6Cl_{16}]^{-10}\}^{-1}\{[La_{11}(SeO_3)_{12}]^{+9}[Cl_8]^{-8}\}^{+1}$ and $\{[Nd_{11}(SeO_3)_{12}]^{+9}[Zn_3Cl_{16}]^{-10}\}^{-1}\{[Nd_{11}(SeO_3)_{12}]^{+9}[Cl_8]^{-8}\}^{+1}$ [11]. Such mixed-layer structures are as yet observed only for selenites; note the compositional shift of the CsCl slabs from $[M^I_7Cl_{16}]^{-9}$ in "bilayer" structures (Figure 1b) to $[M^I_6X_{16}]^{-10}$ in their mixed-layer derivatives [11,53]. In the structures of tellurites, simple "bi-layer" sequences are charge balanced (e.g., $[M^ILn_{11}(TeO_3)_{12}]^{+10}[M^I_6X_{16}]^{-10}$ [10]) and formation of mixed-layer structures is not favored. A very similar pattern was observed in our earlier works on complex layered perovskites [60]. Therefore, if the $[Ln_{11}(SeO_3)_{12}]^{+9}[M^{II}_{7.5}X_{24}]^{-9}$ selenite analogs of the compounds 1–5 discussed here do actually exist, one can foresee also existence of their more complex derivatives such as $\{[Ln_{11}(SeO_3)_{12}]^{+9}[M^{II}_7X_{24}]^{-10}\}^{-1}\{[Ln_{11}(SeO_3)_{12}]^{+9}[X_8]^{-8}\}^{+1}$, etc.

The comparative data on unit cell parameters, space groups, and symmetry relation between different layers in compounds with the general formulas $[Ln_{12}(TeO_3)_{12}][M^{II}_6X_{24}]$, $[(Ln,M^I)_{1-x}Ln_{11}(ChO_3)_{12}][M^I_{6+z}X_{16+y}]$ (Ch = Se or Te), and $[M^{II}Ln_{10}(SeO_3)_{12}][X_8]$ are summarized in Table 2. Other polytypes can be easily obtained using the different combinations of the symmetry operations active in L_{2n} layer.

Table 2. The comparative crystal chemical data on compounds with the general formulas $[Ln_{12}(TeO_3)_{12}][M^{II}_6X_{24}]$, $[(Ln,M^I)_{1-x}Ln_{11}(ChO_3)_{12}][M^I_{6+z}X_{16+y}]$ (Ch = Se or Te), and $[M^{III}Ln_{10}(SeO_3)_{12}][X_8]$ and the character of polytypic relations.

Compound	Sp. Gr.	Symmetry of the Triplet L_{2n-1},L_{2n},L_{2n+1}	Symmetry Operation Active in L_{2n} Layer	Unit Cell Parameters			V, Å^3	Ref.
				a, Å	b, Å	c, Å		
MDO1-polytype								
$[La_{12}(TeO_3)_{12}][Cd_6Cl_{24}]$	*P*4/*nbm*	*P*(4/*n*)*bm*	2_x, 2_y	16.401	16.401	12.918	3474.77	[17]
$[Sm_{12}(TeO_3)_{12}][Cd_6Cl_{24}]$	*P*4/*nbm*	*P*(4/*n*)*bm*	2_x, 2_y	15.842	15.842	13.079	3282.36	[16]
$[Eu_{12}(TeO_3)_{12}][Cd_6Cl_{24}]$	*P*4/*nbm*	*P*(4/*n*)*bm*	2_x, 2_y	15.774	15.774	13.113	3262.94	[16]
$[La_{12}(TeO_3)_{12}][Cd_6Br_{24}]$	*P*4/*nbm*	*P*(4/*n*)*bm*	2_x, 2_y	16.439	16.439	13.713	3705.66	[17]
$[Pr_{12}(TeO_3)_{12}][Cd_6Br_{24}]$	*P*4/*nbm*	*P*(4/*n*)*bm*	2_x, 2_y	16.231	16.231	13.771	3627.91	[17]
MDO2-polytype								
$[CsSm_{11}(TeO_3)_{12}][Cs_6Cl_{16}]$	*I*4/*mcm*	*P*(4/*m*)*bm*	2_{1x}, 2_{1y}	15.888	15.888	25.737	6496.45	[10]
$[RbNd_{11}(TeO_3)_{12}][Rb_6Br_{16}]$	*I*4/*mcm*	*P*(4/*m*)*bm*	2_{1x}, 2_{1y}	16.118	16.118	25.935	6737.51	[10]
$[Sm_{11.397}(TeO_3)_{12}][K_{5.809}Cl_{16}]$	*I*4/*mcm*	*P*(4/*m*)*bm*	2_{1x}, 2_{1y}	15.894	15.894	24.885	6287	[15]
$[Gd_{11.86}(TeO_3)_{12}][K_{4.42}Cl_{16}]$	*I*4/*mcm*	*P*(4/*m*)*bm*	2_{1x}, 2_{1y}	15.804	15.804	24.961	6234	[15]
$[Ho_{11.697}(TeO_3)_{12}][K_{4.908}Cl_{16}]$	*I*4/*mcm*	*P*(4/*m*)*bm*	2_{1x}, 2_{1y}	15.826	15.826	24.817	6216	[15]
$[Pr_{11.781}(TeO_3)_{12}][K_{5.657}Cl_{17}]$	*I*4/*mcm*	*P*(4/*m*)*bm*	2_{1x}, 2_{1y}	16.071	16.071	24.862	6421	[15]
$[Gd_{12}(TeO_3)_{12}][Cd_6Cl_{24}]$	*I*4/*mcm*	*P*(4/*m*)*bm*	2_{1x}, 2_{1y}	15.763	15.763	26.410	6561.82	[15]
$[LiPr_{11}(SeO_3)_{12}][Rb_6Cl_{16}]$	*I*4/*mcm*	*P*(4/*m*)*bm*	2_{1x}, 2_{1y}	15.906	15.906	24.790	6271.89	[13]
$[LiNd_{11}(SeO_3)_{12}][Rb_6Cl_{16}]$	*I*4/*mcm*	*P*(4/*m*)*bm*	2_{1x}, 2_{1y}	15.817	15.817	24.770	6196.90	[12]
MDO3-polytype								
$[CaNd_{10}(SeO_3)_{12}][Cl_8]$ *	*Bbab*	*Pba*(*b*)	2_{1x}, 2_y	15.681	15.588	17.419	4257.82	[52]
$[SrNd_{10}(SeO_3)_{12}][Cl_8]$ *	*Bbab*	*Pba*(*b*)	2_{1x}, 2_y	15.773	15.836	17.622	4401.64	[52]
$[Cs_{0.5}Nd_{10.5}(SeO_3)_{12}][Br_8]$	*Bbab*	*Pba*(*b*)	2_{1x}, 2_y	15.797	15.797	17.693	4482.58	[55]

MDO4-polytype								
$[Nd_{11}(SeO_3)_{12}][Cs_7Cl_{16}]$	*Pna*2$_1$	*P*12/*a*(1)	2$_y$	15.911	15.951	25.860	6563.17	[38]
$[Sm_{11}(SeO_3)_{12}][K_7Cl_{16}]$	*Pnan*	*P*12/*a*(1)	2$_y$	15.633	15.664	25.075	6140.25	[54]
Non-MDO polytypes and modular structures								
$[CsPr_{11}(SeO_3)_{12}][Cs_7Cl_{16}]$ *	*Aeam*	n.d.	n.d.	15.999	15.986	51.698	13222.28	[54]
$[Nd_{11}(SeO_3)_{12}][Cs_7Cl_{16}]$	*Pban*	n.d.	n.d.	15.941	15.954	51.656	13137.29	[38]
$\{[La_{11}(SeO_3)_{12}][Cs_6Cl_{16}]\}$	*Aeam*	*P*(4/*m*)*bm*	2$_{1x}$, 2$_{1y}$	16.073	16.037	43.176	11129.16	[53]
$\{[La_{11}(SeO_3)_{12}][Cl_8]\}$ *		*Pba*(*b*)	2$_{1x}$, 2$_y$					

* The initial unit cell parameters and the space groups have been transformed to preserve the orientation and stacking direction of the OD layers and modules; n.d., no data.

4. Discussion

4.1. Synthesis

In line with our expectations, the family of layered rare-earth chalcogenite halides could be more or less successfully extended into the realm of transition-metal compounds. As yet, the generally employed self-flux synthetic pathway (the use of metal halides as both reactants and fluxing agents) is quite effective in producing single crystals of selenites but essentially less so in the case of tellurites; we estimate the probability of preparing suitable single crystals from a single synthetic run to be as low as 20–30%. The possible explanation is that the targeted tellurites are less soluble in the molten fluxes compared to the selenites. The quality of the produced tellurite crystals is also essentially lower in contrast to selenites. This is the reason why most isostructural series are only sparsely characterized, i.e., structures have been determined for certain members only. This approach also does not provide phase-pure samples. The most common byproduct is microcrystalline TeO_2 which, in the case of alkali fluxes, is generated due to a side reaction yielding hexahalotellurites and their subsequent hydrolysis upon flux leaching. An alternative chemical vapor approach, which works well for structurally related bismuth selenite halides [61], does not work for rare earths due to much lower volatility of their compounds. Yet, the use of reactive MnX_2 and CoX_2 fluxes permitted to prepare the first representatives of two new series of rare-earth-manganese and cobalt tellurite halides.

4.2. Structural Trends

All the compounds reported here adopt the arrangement reported previously by us for the $[Ln_{12}(TeO_3)_{12}][Cd_6X_{24}]$ compounds (X = Cl, Br) [16,17]. This is not surprising, as the MnX_2 and CoX_2 halides adopt related layered structure type with octahedral coordination of the dication [62–66]. No analogs of the $[MLn_{10}(SeO_3)_{12}][X_8]$ [52] or $[Nd_{11}(SeO_3)_{12}]_2[Cl_8][Zn_3Cl_{16}]$ [11] are as yet known among tellurite halides. In the meantime, selenite analogs of the compounds reported here are also unknown. No mixed-layer structures, known among selenites [11], have been reported among tellurites, as these mixed-layer structures contain the $[(M,Ln)_{11+x}(ChO_3)_{12}][X_8]$ (Ch = chalcogen) layer sequence. By now, the only "intersection point" between the tetragonal (or pseudotetragonal) tellurite and selenite halides is the structure depicted in Figure 1b, which contains CsCl-derived metal-halide slabs.

The structure of the metal-tellurite $[Ln_{12}(TeO_3)_{12}]^{12+}$ slabs remains nearly the same in all structures reported herein and in [10–17] and are composed by three types of the sheets: the LnO_8 and LnO_{10} polyhedra share edges and vertices to form an "inner" metal-oxide sheet decorated by the TeO_3 squashed tetrahedra and LnO_4X_4 tetragonal antiprisms ("outer" sheet; Figure 2). Refinement of these parts of the structures proceeds relatively smoothly; they exhibit the best ordering and can be considered structure-directing. The structure of **1** is analogous to those of the other early rare-earth-cadmium compounds and adopts the same *P*4/*nbm* space group with c~13 Å and one cationic and one anionic slab per unit cell (Figure 1d). As we noted earlier in [16], there exists a considerable mismatch

between the size of the layer comprised from regular $CdCl_6$ octahedra (estimated subcell parameter of ~3.75 Å) and the cerium-tellurite slab ($a/4$ = 4.08Å), which can somewhat be compensated by deformations of the octahedral layer; yet some disorder is already invoked. This discrepancy increases sharply when passing from Cd^{2+} ($^{[6]}r$ = 0.95 Å) to Mn^{2+} ($^{[6]}r$ = 0.83 Å) and further to Co^{2+} ($^{[6]}r$ = 0.75 Å) [67]. In these cases, the distortions are already unable to compensate the adjustment of the metal-halide to the metal-oxide slab. Local deviations from the ideal structure which permit either to preserve the acceptable M–X distances or to adapt some M^{2+} cations in tetrahedral coordination are very likely to be present. Unfortunately, only an averaged and statistical picture can be extracted from the single-crystal X-ray data; the observed disorder can otherwise reflect just the overlapping contributions from various "islands" with different M–X arrangements. One may suggest that these discrepancies might decrease when passing from MCl_6 to larger MBr_6 octahedra; however, it is likely to be overruled by the swelling of the unit cell in the ***ab*** plane. It is also worth noting that while a polytypic-like transition from *P*4/*nbm* to *I*4/*mcm* occurs in the $[Ln_{12}(TeO_3)_{12}][Cd_6Cl_{24}]$ series with the borderline between Eu and Gd compounds, no such transition occurs between **4** and **5**. It is, therefore, possible that among compounds of Mn and Co, this transition occurs smoothly and the OD character of the structure is represented by more or less thick lamellae of both *P*4/*nbm* and *I*4/*mcm* layer sequences. It is also rather likely that the compound mentioned in [11] as $[La_{11}(SeO_3)_{12}][Co_{7.5}Cl_{24}]$ also exhibited strong disorder in the metal-halide part of the structure, which could not be plausibly modeled and was thus abandoned. Overall, it should be noted that while metal-halide layers containing magnetically active transition metal cations can indeed be incorporated into the structures of layered rare-earth chalcogenite halides, they form strongly disordered sublattices which are unlikely to result in magnetic ordering.

We also note that by now, the $[Ln_{12}(TeO_3)_{12}][M_6X_{24}]$ compounds have been obtained for the M^{2+} cations characterized by zero (Mn^{2+}, Cd^{2+}) or relatively low (Co^{2+}) values of crystal field stabilization energy (CFSE) which permit essential distortions of their octahedral environment. One can suggest that it is also possible to introduce non-magnetic Mg^{2+}, of the size similar to Co^{2+} ($^{[6]}r$ = 0.72 Å [67]) also characterized by CFSE = 0 (as there are no *d* orbitals), into the structures reported here.

5. Conclusions

To summarize, we succeeded in further developing the layered rare-earth tellurite-halide family by introducing, for the first time, magnetically active transition metal cations into the halide blocks. Despite essential variation of their size, these cations tend to keep the octahedral environment of halide anions; the geometrical mismatch between the cationic and anionic layer can be, more or less effectively, compensated by the increasing degree of disorder in the transition metal sublattice. This disorder increases essentially also when passing from chlorides to bromides, which is in line with the fact that no tellurite iodide featuring the $[(M,Ln)_{11}(TeO_3)_{12}]$ layers has been reported so far. It is more or less evident from this study that further directions of developing this family are possible; however, there is yet little hope in the pursuit of magnetic properties. Other properties related to the type of polytypic structures, including ionic exchange and trapping or soft-chemistry transformations (under mild conditions), might, however, be of interest.

Supplementary Materials: The following supporting information can be downloaded at: https://www.mdpi.com/article/10.3390/sym14102087/s1, Table S1: Fractional site coordinates (*xyz*), site multiplicities (*Q*), equivalent displacement parameters (U_{eq}, Å^2), and site occupancy factor for four compounds $[Cd_6Cl_{24}][Ce_{12}(TeO)_{12}]$ (**1**), $[Mn_6Cl_{24}][Nd_{12}(TeO)_{12}]$ (**2**), $[Mn_6Br_{24}][La_{12}(TeO)_{12}]$ (**3**), $[Co_6Cl_{24}][Eu_{12}(TeO)_{12}]$ (**4**) and $[Co_6Cl_{24}][Gd_{12}(TeO)_{12}]$ (**5**); Table S2: Selected interatomic distances (Å) for compounds 1–5.

Author Contributions: Conceptualization, D.O.C. and S.M.A.; methodology, V.A.D.; formal analysis, T.A.O., Y.A.V., S.N.V. and D.V.D.; writing—original draft preparation, D.O.C. and S.M.A.; writing—review and editing, D.O.C. and S.M.A. All authors have read and agreed to the published version of the manuscript.

Funding: This research was funded by the Russian Science Foundation, grant number 20–77-10065 (in the part of the analysis of the polytypism and OD relationship) and the state task of Russian Federation, state registration number 122011300125–2].

Conflicts of Interest: The authors declare no conflict of interest.

References

1. Zimmermann, I.; Johnsson, M. A Synthetic Route toward Layered Materials: Introducing Stereochemically Active Lone-Pairs into Transition Metal Oxohalides. *Cryst. Growth Des.* **2014**, *14*, 5252–5259. https://doi.org/10.1021/cg5010374.
2. Johnsson, M.; Lidin, S.; Törnroos, K.W.; Bürgi, H.-B.; Millet, P. Host–Guest Compounds in the Family of Tellurium–Nickel Oxohalogenides. *Angew. Chem. Int. Ed.* **2004**, *43*, 4292–4295. https://doi.org/10.1002/anie.200460001.
3. Ok, K.M. Toward the Rational Design of Novel Noncentrosymmetric Materials: Factors Influencing the Framework Structures. *Acc. Chem. Res.* **2016**, *49*, 2774–2785. https://doi.org/10.1021/acs.accounts.6b00452.
4. Mayerová, Z.; Johnsson, M.; Lidin, S. Lone-Pair Interfaces That Divide Inorganic Materials into Ionic and Covalent Parts. *Angew. Chem. Int. Ed.* **2006**, *45*, 5602–5606. https://doi.org/10.1002/anie.200600861.
5. Zhang, S.-Y.; Hu, C.-L.; Li, P.-X.; Jiang, H.-L.; Mao, J.-G. Syntheses, crystal structures and properties of new lead(ii) or bismuth(iii) selenites and tellurite. *Dalt. Trans.* **2012**, *41*, 9532. https://doi.org/10.1039/c2dt30560g.
6. Sun, C.; Yang, B.; Mao, J. Structures and properties of functional metal iodates. *Sci. China Chem.* **2011**, *54*, 911–922. https://doi.org/10.1007/s11426-011-4289-8.
7. Zheng, T.; Wang, Q.; Ren, J.; Cao, L.; Huang, L.; Gao, D.; Bi, J.; Zou, G. Halogen regulation triggers structural transformation from centrosymmetric to noncentrosymmetric switches in tin phosphate halides Sn_2PO_4X (X = F, Cl). *Inorg. Chem. Front.* **2022**, *9*, 4705–4713. https://doi.org/10.1039/D2QI01207C.
8. Goerigk, F.C.; Schander, S.; Hamida, M.B.; Kang, D.-H.; Ledderboge, F.; Wickleder, M.S.; Schleid, T. Die monoklinen Seltenerdmetall(III)-Chlorid-Oxidoarsenate(III) mit der Zusammensetzung $SE_5Cl_3[AsO_3]_4$ (SE =La–Nd, Sm). *Z. Naturforsch. B* **2019**, *74*, 497–506. https://doi.org/10.1515/znb-2019-0019.
9. Ahlers, R.; Ruschewitz, U. Non-centrosymmetric coordination polymers based on thallium and acetylenedicarboxylate. *Solid State Sci.* **2009**, *11*, 1058–1064. https://doi.org/10.1016/j.solidstatesciences.2009.03.008.
10. Charkin, D.O.; Black, C.; Downie, L.J.; Sklovsky, D.E.; Berdonosov, P.S.; Olenev, A.V.; Zhou, W.; Lightfoot, P.; Dolgikh, V.A. $Cs_7Sm_{11}[TeO_3]_{12}Cl_{16}$ and $Rb_7Nd_{11}[TeO_3]_{12}Br_{16}$, the new tellurite halides of the tetragonal $Rb_6LiNd_{11}[SeO_3]_{12}Cl_{16}$ structure type. *J. Solid State Chem.* **2015**, *232*, 56–61. https://doi.org/10.1016/j.jssc.2015.08.043.
11. Hamida, M.B. Oxo-Selenate(IV) und Oxo-Arsenate(III) der Selten-Erd-Metalle und ihre Derivate. Ph.D. Thesis, Universität Oldenburg, Oldenburg, Germany, 2007.
12. Lipp, C.; Schleid, T. $Rb_6LiNd_{11}Cl_{16}[SeO_3]_{12}$: Ein durch zwei chloridische Flussmittel derivatisiertes Neodym(III)-Oxoselenat(IV). *Z. Fuer Krist.* **2005**, *22*, 165.
13. Lipp, C.; Schleid, T. $Rb_6LiPr_{11}Cl_{16}[SeO_3]_{12}$: Ein chloridisch derivatisiertes Rubidium-Lithium-Praseodym(III)-Oxoselenat(IV). *Z. Für Anorg. Und Allg. Chem.* **2006**, *632*, 2226–2231. https://doi.org/10.1002/zaac.200600126.
14. Zitzer, S.; Lipp, C.; Schleid, Th. Two isostructural alkali-metal europium chloride oxochalcogenates: $Rb_6LiEu_{11}Cl_{16}[SeO_3]_{12}$ versus $Cs_7Eu_{11}Cl_{16}[TeO_3]_{12}$. In Proceedings of the European Conference on Solid State Chemistry (ECSCC); Lund, Sweden, September 25–28, 2011; p. 71.
15. Charkin, D.O.; Volkov, S.N.; Dolgikh, V.A.; Aksenov, S.M. Potassium rare-earth tellurite chlorides: A new branch from the old root. *Solid State Sci.* **2022**, *129*, 106895. https://doi.org/10.1016/j.solidstatesciences.2022.106895.
16. Kharitonov, I.D.; Charkin, D.O.; Berdonosov, P.S.; Black, C.; Downie, L.J.; Lightfoot, P.; Dolgikh, V.A. Rare-Earth Cadmium Tellurite Chlorides with a Structural Type Exhibiting $[Ln_{12}(TeO_3)_{12}]$ Slabs Alternating with $CdCl_6$ Octahedral Layers. *Eur. J. Inorg. Chem.* **2014**, *2014*, 3140–3146. https://doi.org/10.1002/ejic.201402177.
17. Charkin, D.O.; Grishaev, V.Y.; Volkov, S.N.; Dolgikh, V.A. Synthesis and Structure of New Rare Earth Cadmium Tellurite Halides. *Russ. J. Inorg. Chem.* **2020**, *65*, 466–471. https://doi.org/10.1134/S0036023620040038.
18. Ferraris, G.; Makovicky, E.; Merlino, S. *Crystallography of Modular Materials*; Oxford University Press: Oxford, UK, 2008.
19. Zvyagin, B.B. Polytypism of crystal structures. *Comput. Math. Appl.* **1988**, *16*, 569–591. https://doi.org/10.1016/0898-1221(88)90247-7.
20. Fichtner, K. Order-disorder structures. *Comput. Math. Appl.* **1988**, *16*, 469–477. https://doi.org/10.1016/0898-1221(88)90237-4.
21. Ďurovič, S.; Hybler, J. OD structures in crystallography—basic concepts and suggestions for practice. *Z. Krist. Cryst. Mater.* **2006**, *221*, 63–76. https://doi.org/10.1524/zkri.2006.221.1.63.

22. Dornberger-Schiff, K.; Fichtner, K. On the Symmetry of OD-Structures Consisting of Equivalent Layers. *Krist. Technol.* **1972**, *7*, 1035–1056. https://doi.org/10.1002/crat.19720070907.
23. Dornberger-Schiff, K. Grundzüge einer Theorie der OD-Strukturen aus Schichten. Abhandlungen der Dtsch. *Akad. Der Wiss. Zu Berlin. Kl. Chem. Geol. Biol.* **1964**, 3, 107.
24. Fichtner, K. On the Description of Symmetry of OD Structures (I) OD Groupoid Family, Parameters, Stacking. *Krist. Technol.* **1979**, *14*, 1073–1078. https://doi.org/10.1002/crat.19790140907.
25. Grell, J. Symmetry Description of OD Crystal Structures in Group Theoretical Terms. *Acta Appl. Math.* **1998**, *52*, 261–269. https://doi.org/10.1023/a:1005939931744.
26. Stöger, B. Non-Crystallographic Layer Lattice Restrictions in Order-Disorder (OD) Structures. *Symmetry* **2014**, *6*, 589–621. https://doi.org/10.3390/sym6030589.
27. Nespolo, M.; Durovic, S. Crystallographic basis of Polytypism and Twinning in Micas. *Rev. Mineral. Geochem.* **2002**, *46*, 155–279. https://doi.org/10.2138/rmg.2002.46.04.
28. Topnikova, A.; Belokoneva, E.; Dimitrova, O.; Volkov, A.; Deyneko, D. $Rb_{1.66}Cs_{1.34}Tb[Si_{5.43}Ge_{0.57}O_{15}]\cdot H_2O$, a New Member of the OD-Family of Natural and Synthetic Layered Silicates: Topology-Symmetry Analysis and Structure Prediction. *Minerals* **2021**, *11*, 395. https://doi.org/10.3390/min11040395.
29. Belokoneva, E.L.; Topnikova, A.P.; Aksenov, S.M. Topolology-symmetry law of structure of natural titanosilicate micas and related heterophyllosilicates based on the extended OD theory: Structure prediction. *Crystallogr. Rep.* **2015**, *60*, 1–15. https://doi.org/10.1134/S1063774515010058.
30. Belokoneva, E.L. Borate crystal chemistry in terms of the extended OD theory: Topology and symmetry analysis. *Crystallogr. Rev.* **2005**, *11*, 151–198. https://doi.org/10.1080/08893110500230792.
31. Reutova, O.; Belokoneva, E.; Volkov, A.; Dimitrova, O. Structure-Properties Relations in Two Iodate Families Studied by Topology-Symmetry Analysis of OD Theory. *Symmetry* **2021**, *13*, 1477. https://doi.org/10.3390/sym13081477.
32. Reutova, O.; Belokoneva, E.; Volkov, A.; Dimitrova, O.; Stefanovich, S. Two New $Rb_3Sc(IO_3)_6$ Polytypes in Proposed Nonlinear Optical Family $A_3M(IO_3)_6$ (A = K, Rb; M = Sc, In): Topology–Symmetry Analysis, Order–Disorder and Structure–Properties Relation. *Symmetry* **2022**, *14*, 1699. https://doi.org/10.3390/sym14081699.
33. Aksenov, S.; Antonov, A.; Deyneko, D.; Krivovichev, S.; Merlino, S. Polymorphism, polytypism and modular aspect of compounds with the general formula $A_2M_3(TO_4)_4$ (A = Na, Rb, Cs, Ca; M = Mg, Mn, Fe^{3+}, Cu^{2+} ; T = S^{6+}, P^{5+}): Order–disorder, topological description and DFT calculations. *Acta Crystallogr. Sect. B Struct. Sci. Cryst. Eng. Mater.* **2022**, *78*, 61–69. https://doi.org/10.1107/S2052520621009136.
34. Aksenov, S.M.; Kuznetsov, A.N.; Antonov, A.A.; Yamnova, N.A.; Krivovichev, S.V.; Merlino, S. Polytypism of Compounds with the General Formula $Cs\{Al_2[TP_6O_{20}]\}$ (T = B, Al): OD (Order-Disorder) Description, Topological Features, and DFT-Calculations. *Minerals* **2021**, *11*, 708. https://doi.org/10.3390/min11070708.
35. Stöger, B.; Krüger, H.; Weil, M. $Mg(H_2O)_2$ $[TeO_2(OH)_4]$: A polytypic structure with a two-mode disordered stacking arrangement. *Acta Crystallogr. Sect. B Struct. Sci. Cryst. Eng. Mater.* **2021**, *77*, 605–623. https://doi.org/10.1107/S2052520621006223.
36. Stöger, B.; Weil, M.; Missen, O.P.; Mills, S.J. The Order-Disorder (OD) Polytypism of $[Cu_2ZnTeO_4]^{2+}[SO4\cdot H2O]^{2-}$. *Cryst. Res. Technol.* **2020**, *55*, 1900182. https://doi.org/10.1002/crat.201900182.
37. Eder, F.; Stöger, B.; Weil, M. Order-disorder (OD) structures of $Rb_2Zn(TeO_3)(CO_3)\cdot H_2O$ and $Na_2Zn_2Te_4O_{11}$. *Z. Krist. Cryst. Mater.* **2022**, *237*, 329–341. https://doi.org/10.1515/zkri-2022-0030.
38. Berdonosov, P.S.; Akselrud, L.; Prots, Y.; Abakumov, A.M.; Smet, P.F.; Poelman, D.; Van Tendeloo, G.; Dolgikh, V.A. $Cs_7Nd_{11}(SeO_3)_{12}Cl_{16}$: First Noncentrosymmetric Structure among Alkaline-Metal Lanthanide Selenite Halides. *Inorg. Chem.* **2013**, *52*, 3611–3619. https://doi.org/10.1021/ic301442f.
39. Oxford Diffraction. CrysAlisPro; Oxford Diffraction Ltd: Abingdon, UK, 2009.
40. Bruker. SAINT. Bruker AXS Inc.: Madison, Wisconsin, USA, 2012.
41. Bruker. SADABS. Bruker AXS Inc.: Madison, Wisconsin, USA, 2001.
42. Palatinus, L.; Chapuis, G. Superflip—A computer program for the solution of crystal structures by charge flipping in arbitrary dimensions. *J. Appl. Crystallogr.* **2007**, *40*, 786–790. https://doi.org/10.1107/S0021889807029238.
43. Petricek, V.; Dusek, M.; Palatinus, L. Crystallographic Computing System JANA2006: General features. *Z. Fuer Krist.* **2014**, *229*, 345–352.
44. Brandenburg, K.; Putz, H. *Diamond Version 3*; Crystal Impact GbR.: Bonn, Germany, 2005.
45. Prince, E. (Ed.). *International Tables for Crystallography, Mathematical, Physical and Chemical Tables*, 3rd ed.; Wiley: Hoboken, NJ, USA, 2004; Volume C.
46. Merlino, S. (Ed.). *EMU Notes in Mineralogy. Modular Aspects of Minerals*; Eötvös University Press: Budapest, Hungary, 1997; Volume 1.
47. Dornberger-Schiff, K. On order–disorder structures (OD-structures). *Acta Crystallogr.* **1956**, *9*, 593–601. https://doi.org/10.1107/S0365110X56001625.
48. Dornberger-Schiff, K. OD Structures—a Game and a Bit More. *Krist. Technol.* **1979**, *14*, 1027–1045. https://doi.org/10.1002/crat.19790140903.

49. Dornberger-Schiff, K.; Grell, H. Geometrical properties of MDO polytypes and procedures for their derivation. II. OD families containing OD layers of M > 1 kinds and their MDO polytypes. *Acta Crystallogr. Sect. A* **1982**, *38*, 491–498. https://doi.org/10.1107/S0567739482001053.
50. Dornberger-Schiff, K. On the nomenclature of the 80 plane groups in three dimensions. *Acta Crystallogr.* **1959**, *12*, 173–173. https://doi.org/10.1107/S0365110X59000482.
51. Grell, H.; Dornberger-Schiff, K. Symbols for OD groupoid families referring to OD structures (polytypes) consisting of more than one kind of layer. *Acta Crystallogr. Sect. A* **1982**, *38*, 49–54. https://doi.org/10.1107/S0567739482000096.
52. Berdonosov, P.S.; Olenev, A.V.; Dolgikh, V.A.; Lightfoot, P. The synthesis and crystal structures of the first rare-earth alkaline-earth selenite chlorides $MNd_{10}(SeO_3)_{12}Cl_8$ (M=Ca and Sr). *J. Solid State Chem.* **2007**, *180*, 3019–3025. https://doi.org/10.1016/j.jssc.2007.08.019.
53. Berdonosov, P.S.; Oleneva, O.S.; Dolgikh, V.A. Tricaesium undecalanthanum dodecaselenate(IV) dodecachloride. *Acta Crystallogr. Sect. E Struct. Rep. Online* **2006**, *62*, i29–i31. https://doi.org/10.1107/S1600536806002042.
54. Berdonosov, P.S.; Dolgikh, V.A.; Schmidt, P.; Ruck, M. Complex chloride-selenites of rare earthes—a family of new phases. In Proceedings of the IV National Crystal Chemical Conference; Chernogolovka, Russia, 26–30 June 2006; pp. 192–193.
55. Ruck, M.; Schmidt, P. Synthesen und Kristallstrukturen der homöotypen Selenitbromide $Bi_8(SeO_3)_9Br_6$ und $CsSm_{21}(SeO_3)_{24}Br_{16}$. *Z. Anorg. Allg. Chem.* **2003**, *629*, 2133–2143. https://doi.org/10.1002/zaac.200300192.
56. Lima-de-Faria, J.; Hellner, E.; Liebau, F.; Makovicky, E.; Parthé, E. Nomenclature of inorganic structure types. Report of the International Union of Crystallography Commission on Crystallographic Nomenclature Subcommittee on the Nomenclature of Inorganic Structure Types. *Acta Crystallogr. Sect. A Found. Crystallogr.* **1990**, *46*, 1–11. https://doi.org/10.1107/S0108767389008834.
57. Veblen, D.R. Polysomatism and polysomatic series: A review and applications. *Am. Mineral.* **1991**, *76*, 801–826.
58. Ferraris, G.; Gula, A. Polysomatic Aspects of Microporous Minerals—Heterophyllosilicates, Palysepioles and Rhodesite-Related Structures. *Rev. Mineral. Geochem.* **2005**, *57*, 69–104. https://doi.org/10.2138/rmg.2005.57.3.
59. Charkin, D.O. Modular approach as applied to the description, prediction, and targeted synthesis of bismuth oxohalides with layered structures. *Russ. J. Inorg. Chem.* **2008**, *53*, 1977–1996. https://doi.org/10.1134/S0036023608130019.
60. Charkin, D.O.; Akinfiev, V.S.; Alekseeva, A.M.; Batuk, M.; Abakumov, A.M.; Kazakov, S.M. Synthesis and cation distribution in the new bismuth oxyhalides with the Sillén–Aurivillius intergrowth structures. *Dalt. Trans.* **2015**, *44*, 20568–20576. https://doi.org/10.1039/C5DT02620B.
61. Aliev, A.; Kovrugin, V.M.; Colmont, M.; Terryn, C.; Huvé, M.; Siidra, O.I.; Krivovichev, S.V.; Mentré, O. Revised Bismuth Chloroselenite System: Evidence of a Noncentrosymmmetric Structure with a Giant Unit Cell. *Cryst. Growth Des.* **2014**, *14*, 3026–3034. https://doi.org/10.1021/cg500293w.
62. Tornero, J.D.; Fayos, J. Single crystal structure refinement of $MnCl_2$. *Z. Krist. Cryst. Mater.* **1990**, *192*, 147–148. https://doi.org/10.1524/zkri.1990.192.14.147.
63. Wollan, E.O.; Koehler, W.C.; Wilkinson, M.K. Neutron Diffraction Study of the Magnetic Properties of $MnBr_2$. *Phys. Rev.* **1958**, *110*, 638–646. https://doi.org/10.1103/PhysRev.110.638.
64. Ferrari, A.; Braibanti, A.; Bigliardi, G. Refinement of the crystal structure of $NiCl_2$ and of unit-cell parameters of some anhydrous chlorides of divalent metals. *Acta Crystallogr.* **1963**, *16*, 846–847. https://doi.org/10.1107/S0365110X6300222X.
65. Wilkinson, M.K.; Cable, J.W.; Wollan, E.O.; Koehler, W.C. Neutron Diffraction Investigations of the Magnetic Ordering in $FeBr_2$, $CoBr_2$, $FeCl_2$, and $CoCl_2$. *Phys. Rev.* **1959**, *113*, 497–507. https://doi.org/10.1103/PhysRev.113.497.
66. Ketelaar, J.A.A. Die Kristallstruktur des Nickelbromids und -jodids. *Z. Krist. Cryst. Mater.* **1934**, *88*, 26–34. https://doi.org/10.1524/zkri.1934.88.1.26.
67. Shannon, R.D. Revised effective ionic radii and systematic studies of interatomic distances in halides and chalcogenides. *Acta Crystallogr. Sect. A* **1976**, *32*, 751–767. https://doi.org/10.1107/S0567739476001551.